Reverse recovery of a GaAs optoelectronic thyristor

V. Korobov[a] and V. Mitin
Department of Electrical and Computer Engineering, Wayne State University, Detroit, Michigan 48202

(Received 29 June 1995; accepted for publication 19 September 1995)

Results of numerical simulation of reverse recovery processes in a two-terminal GaAs optothyristor are presented. In the highly conducting ON state there are many excess carriers in the inner layers of the device. Reversing the anode voltage removes these carriers, turning the device off. The behavior of a *PnpN* structure after reversing the anode voltage essentially depends on the width of the *n* base. For a wide *n* base, negative anode voltage has little effect on carrier removal. In the case of a narrow *n* region, penetration of an electric field into the *p* base is responsible for a fast removal of slowly diffusing holes from the device. This allows decrease in turn-off times by several orders of magnitude over traditional two-terminal devices. The thyristor is switched off completely after the time interval, when all holes have been evacuated from the *p* base. Reverse-recovery time for this regime of ''*n*-base punchthrough'' is calculated in terms of device parameters. © *1996 American Institute of Physics.* [S0021-8979(96)09301-X]

I. INTRODUCTION

Recently, there has been a growing interest in optoelectronic thyristor-like light-emitting semiconductor devices based on III–V direct band-gap semiconductor structures.[1–6] These bistable devices have two distinct electrical and optical states. In the OFF state their resistance is high and no optical emission occurs, while in the ON state the devices emit light and exhibit low impedances. Transition between the two states is induced by either an optical or an electrical input, making it possible to use them as optoelectronic switches.[1,3] Other applications include optical amplifiers,[7] optoelectronic integrated circuits and elements of dynamic optoelectronic memory,[8] negative differential resistance lasers,[9] laser/laser drivers, etc. Many of these applications require high speed. While gallium arsenide thyristors demonstrated fast subnanosecond turn-on (with switching times below 300 ps),[10] the low turn-off speed is still a serious problem. During device operation in the ON state, carrier concentrations in the central *n* and *p* layers of a thyristor are much higher than in equilibrium. In order to switch the device off, excess carriers, supporting the ON state, have to be reduced below the holding level. Otherwise, a small increase of the anode voltage V_A rapidly switches the thyristor on due to the so-called dV/dt switching.[11] Attempts to remove excess carriers by reversing the anode voltage have not been successful. It was reported[8] that several microseconds were required for an excess charge to reach equilibrium after applying a negative anode voltage to the two-terminal device, which initially operated in the ON state.

A well-known method of handling this problem is to use gates, attached directly to the bases of a thyristor. The gate turn off of GaAs thyristors demonstrated a high-speed response of the order of 2 ns[12] because both excess holes and electrons are swept out into the gates by an electric field. Gated thyristors are technologically more complicated than two-terminal devices. For such applications as integration of thyristors into large two-dimensional arrays,[13] only two-terminal devices without gates may be used. The fast recovery of *PnpN* structures could essentially expand their applications for optical parallel processing, copying, and transmission of optical images.

Here we present results of numerical simulation of reverse recovery processes in a GaAs optoelectronic thyristor. While numerous calculations have been presented on Si-based power thyristors, little has been done for GaAs-based *PnpN* structures. [We use the notations *P* and *N* for the heavily doped outer regions (emitters), and *n* and *p* for lightly doped inner regions (bases)]. To date there has been little research done on direct simulation of four-layer *PnpN* optical switches.[15] The main attention in Ref. 15 was paid to the effects of optical generation and carrier lifetimes on dc current–voltage characteristics of the switches. Reverse recovery processes of GaAs optothyristors have not been published yet.

The main emphasis of our article is the analysis of recovery processes in optothyristors, when the *n* base becomes punched through after applying a negative anode voltage. This recovery process allows one to decrease switching times of two-terminal devices simply by applying a negative anode voltage to the anode of an optothyristor. Knowledge of recovery times is important for the design of fast optoelectronic switches.[13] The highest operating frequency is also limited by the recovery time.[16] An expression for a recovery time in terms of device parameters has been derived via an analysis of our simulation results.

Formulation of the numerical approach is given in Sec. II. Simulation results are presented in Sec. III. The effects of device geometry on the rate of carriers removal as well as on the immunity with respect to dV/dt switching are discussed.

II. NUMERICAL APPROACH

The semiconductor device equations we solved are Poisson's equation for electrostatic potential ψ

$$F_1(\xi)=\nabla\cdot\epsilon\nabla\psi-q(n-p+N_A-N_D)=0 \tag{1}$$

[a]Electronic mail: korobov@ciao.eng.wayne.edu

and time-dependent current continuity equations for electron and hole concentrations n and p:

$$F_2(\xi)=\frac{\partial n}{\partial t}-\nabla\cdot\frac{J_n}{q}-R(n,p)+G=0, \tag{2}$$

$$F_3(\xi)=\frac{\partial p}{\partial t}+\nabla\cdot\frac{J_p}{q}-R(n,p)+G=0. \tag{3}$$

Here J_n and J_p are electron and hole current densities, N_A and N_D donor and acceptor concentrations, q is electron charge, and G is the rate of optical generation. ξ is a group of variables, consisting of n,p, and ψ. The recombination term in Eqs. (2) and (3) accounts for three major mechanisms of generation recombination: band-to-band radiative recombination $R_{\rm sp}$, Hall–Shockley–Read $R_{\rm HSR}$ and Auger $R_{\rm Aug}$ terms:

$$R(n,p)=R_{\rm sp}+R_{\rm HSR}+R_{\rm Aug}, \tag{4}$$

$$R_{\rm sp}=B_0(np-n_i^2), \tag{5}$$

$$R_{\rm HSR}=\frac{np-n_i^2}{\tau_1(n+n_1)+\tau_2(p+p_1)}, \tag{6}$$

$$R_{\rm Aug}=(C_1n+C_2p)(np-n_i^2). \tag{7}$$

Here n_i stands for intrinsic carrier concentration in GaAs, $B_0=7.7\times10^{-10}$ cm^3/s is the spontaneous recombination coefficient.[17] Parameters of the HSR recombination are $\tau_n=\tau_p=5\times10^{-7}$ s and $n_1=p_1=n_i$, the intrinsic concentration. Using these values, we assume that the device is of a high quality and the recombination through deep defect levels is not a major recombination process. $R_{\rm sp}$ gives the main contribution to the total recombination term $R(n,p)$ in Eq. (4). The impact ionization mechanism is not included in the current simulator because, as will be seen from our results, this effect is not important in the range of applied reverse voltages under considerations. Temperature is assumed to be 300 K.

The box integration method[18] has been used to discretize the Poisson's equation. A Sharfetter–Gummel scheme[19] has been implemented for the discretization of the drift-diffusion continuity equations. A fully implicit finite difference scheme generates a nonlinear system of discrete equations, which has been solved by Newton–Raphson method.[18] The independent variables for differentiation were chosen to be hole and electron densities p and n, and electrostatic potential ψ. The solution at the previous moment of time was always used as an initial guess to get a solution at the next time moment. The Yale Sparse Matrix Solver[20] has been used for the inversion of the Jacobian matrix at each iteration step.

III. RESULTS AND DISCUSSION

To analyze the reverse recovery of an optothyristor, we simulate transient processes after a negative anode voltage is applied to the device, which operates in the ON state. First of all we find a stationary solution of Eqs. (1)–(3), corresponding to the ON state.

To go from the OFF to the ON state we did the following. Starting from equilibrium, we incremented voltage to get stationary carrier and potential distributions in the forward blocking mode. Generation term G in Eq. (4) is equal to zero. Under these conditions there occurs a large voltage drop across the middle pn junction and small current density. To switch the device on, we assume that thyristor has been activated by light. It means that at the moment of time $t=0$ the generation term $G\neq0$ is added to the expression (4) and a relaxation period starts. Optical carrier generation has no significant effect on carrier distribution and current density in the ON state. Because the ON state of thyristor is self-supporting, after some interval of time we can turn light off, and the device remains in the highly conducting state. After a transient decay, the stationary solution, corresponding to a highly conducting state at some forward bias was obtained. This procedure was found to be very efficient for "preparation" of the initial state.

After the steady ON state is reached the anode voltage is reversed at $t=0$. We will consider two structures. Structure I consists of two outer regions (P and N) doped with 10^{17} cm^{-3}, and inner regions (p and n) equally doped with 10^{15} cm^{-3}. Widths of P,n,p, and N layers are 2.5, 7.5, 5, and 2 μm, respectively. Structure II has the same doping profile, but n-base width for the second device is five times smaller than for the structure I (1.5 μm), p-base width remains the same (5 μm). The sizes of the heavily doped P and N regions are 3.5 and 3 μm. Total length of the device II is 13 μm. We will refer to structures I and II as to structures with "wide" and "narrow" bases, respectively.

A. "Wide" *n* base

Initially device I operated in the ON state with a current density 795 A/cm^2 and a forward voltage drop 1 V. Figure 1 shows potential and carrier distributions for the structure I in the ON state. From Fig. 1(a) we can see that there is practically no potential barrier near the middle pn junction at $x=10$ μm. A dashed line shows equilibrium distribution of electrostatic potential; anode (located at $x=0$) was assumed to be grounded. Figure 1(b) shows that there exists a quasineutrality in the inner regions, where carrier concentrations are almost equal to each other: $n(x)\approx p(x)\approx2.5\times10^{16}$ cm^{-3}. It means that device operates at a high injection level, i.e., electron and hole concentrations are much greater than background doping concentrations 10^{15} cm^{-3} in both bases.

At the moment of time $t=0$ the external circuit is switched to a reverse bias and a negative voltage V is applied to the anode. Current immediately changes its direction of flow and current decay is shown in Fig. 2. Curves 1 and 2 show the total particle currents versus time for $V=-1$ V and $V=-6$ V. It is seen, that reverse current is not a strong function of applied voltage for all moments of time except for a very short time interval (<0.05 ns), when a displacement current is essential.

When anode voltage became negative, electrons from the center n and p regions go to the right, reach the pN junction and are dragged out by the field of the reverse biased junction to the cathode. This current flow does not cause the decrease of electron concentration in the center of the device, because the total number of electrons leaving some region is compensated by the same number of elec-

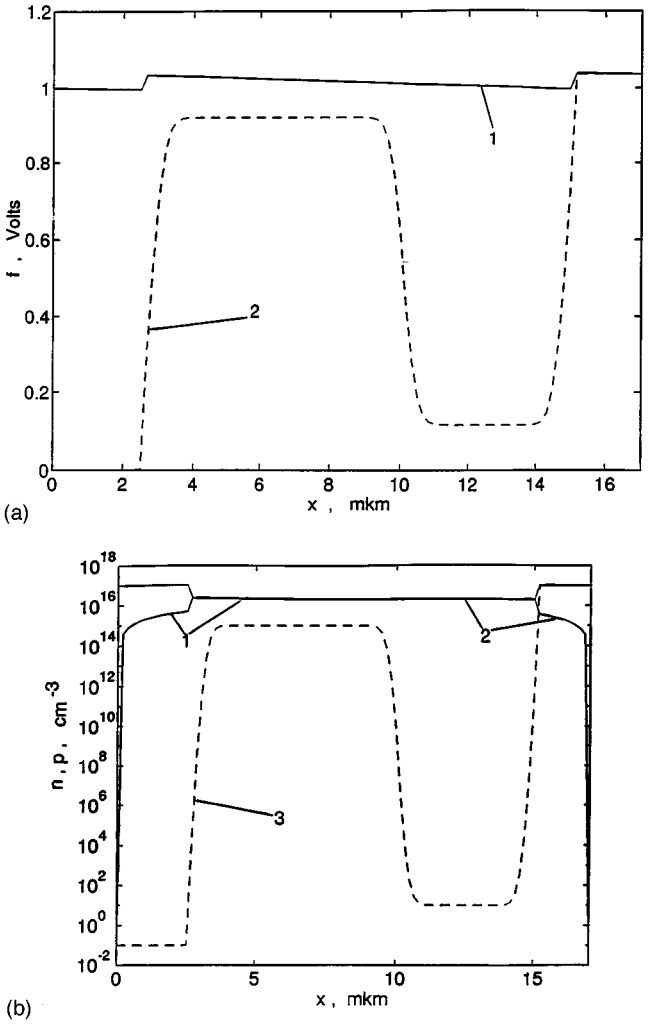

FIG. 1. Potential and carrier distributions along *PnpN* structure I. Dopings of *P* and *N* outer regions are 10^{17} cm^{-3}; *p* and *n* bases have dopings 10^{15} cm^{-3}. *Pn*,*np*, and *nP* junctions are at $x=2.5$ μm, $x=9$ μm, and $x=15$ μm. (a) Distribution of potential in the ON state at forward bias 1 V (curve 1). Curve 2 shows equilibrium potential plot. (b) Curve 1 and 2 represent electron and hole densities for the same structure at forward bias 1 V. In inner regions carrier concentrations are much greater than concentrations of dopants (10^{15} cm^{-3}). Dashed line 3 shows equilibrium electron distribution.

trons coming to the region. Decrease of electrons concentration takes place only near the *Pn* junction. Here electrons have been carried off to the right and they have not been replaced from the left, because the amount of electrons in the *P* emitter is negligible. The decrease of electrons concentrations here gives rise to a space-charge region, where electric field starts to build up. As can be seen from the Fig. 3 the development of the depletion region with high electric field stops at the moment of time $t\approx 0.25$. At the same time no depletion region has been formed near the *pN* junction, where the electric field is close to the equilibrium value. The asymmetry is due to the different diffusivities of electrons and holes in GaAs.

After the depletion region has been built up near the *Pn* junction, the next stage of relaxation starts, when the electric field's magnitude changes little, and the carrier concentrations slowly decrease with time. As electron and hole distributions show (Fig. 4), outside the depletion region the neu-

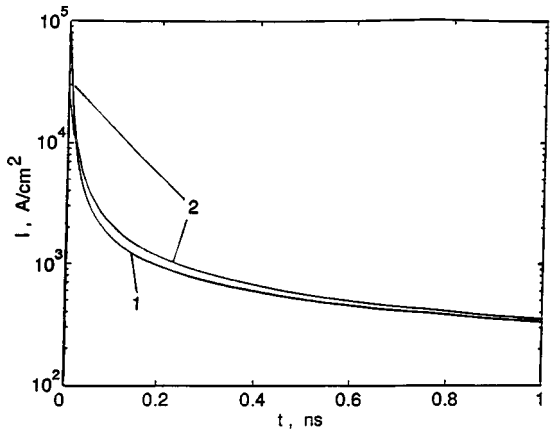

FIG. 2. Time variation of the total electric current through structure I for voltages, pulsed at $t=0$ from 1 to -1 V (curve 1) and from 1 to -6 V (curve 2).

tral region still exists, where charge neutrality is maintained due to equal numbers of electrons and holes. In the space-charge region the number of electrons is negligible, and the total charge is simply the charge of uncompensated donors with concentration N_D (number of remaining holes is much smaller than N_D). Neglecting the contribution of the mobile charge we can write for the electric field $E(x)$ in the *n* region near the *Pn* junction:

$$E(x)=\frac{4\pi q}{\epsilon}N_D(x-a), \tag{8}$$

where a, the width of the space-charge region, can be found as $a=\sqrt{\epsilon V/2\pi qN_D}$. Calculation for $V=6$ V gives $a=0.26\times 10^{-3}$ cm, what corresponds to Fig. 3.

Figure 5 shows current distributions of electrons and holes at two different moments of time $t=4.5$ ns and $t=14$ ns. The sum of electron j_n and hole j_p currents is practically

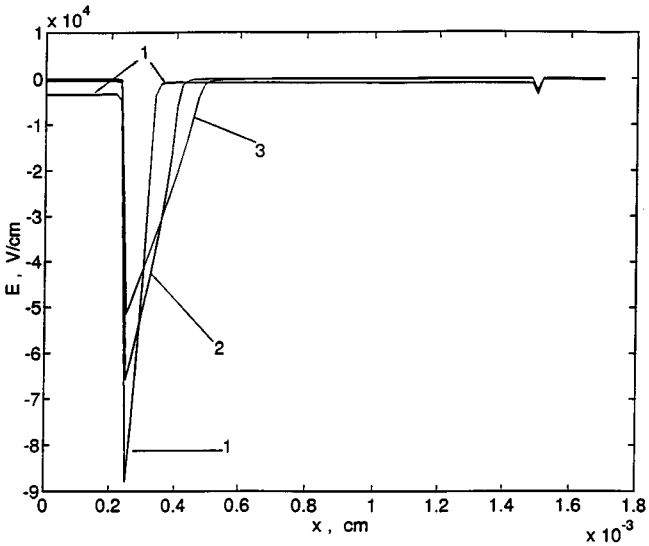

FIG. 3. Electric field in structure I at different moments of time *t* after reversing voltage from 1 to -6 V at $t=0$. (1) $t=0.05$ ns, (2) $t=1$ ns, (3) $t=2.5$ ns. After $t=2.5$ ns distribution of electric field practically does not change with time.

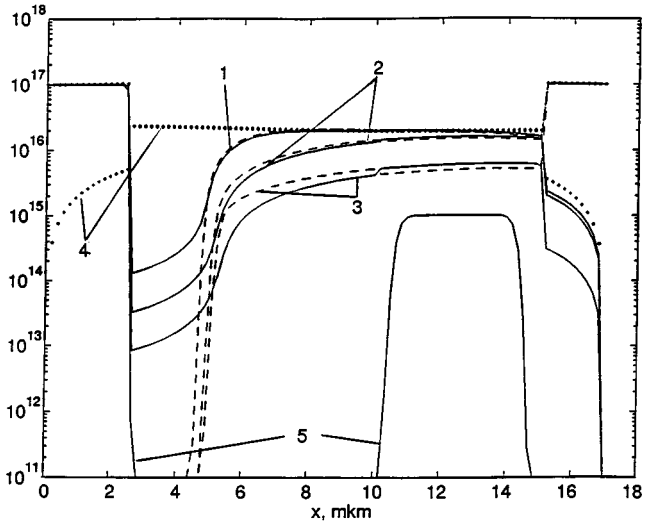

FIG. 4. Hole (solid lines) and electrons (dashed lines) at different time moments t for structure I: (1) $t=4.5$ ns, (2) $t=14$ ns, (3) $t=100$ ns. In the space-charge region (between $x=2.6$ μm and $x=4.5$ μm) electron concentration is negligible. Hole concentration here is larger because holes, swept out to the P emitter (located at $x<2\mu$m), are replaced from the right. Nevertheless, hole density in this region can be neglected in comparison with donor concentration $N_D=10^{15}$ cm^{-3}. Dotted line 4 corresponds to the electron distribution for a steady ON state. Equilibrium hole concentration (curve 5) is also shown for a comparison.

constant through the whole device, so displacement current is negligible. In the space-charge region electron concentration is negligible and the total current $j(t)$ is controlled by holes. It can be written as

$$j(t)\approx q\mu_p p(x,t)E(x,t). \tag{9}$$

For arbitrary moment of time hole concentration can be expressed as

$$p(x,t)=\frac{j(t)}{q\mu_p E(x,t)}=\frac{j(t)}{\mu_p(4\pi q^2/\epsilon)N_D(x-a)}\,. \tag{10}$$

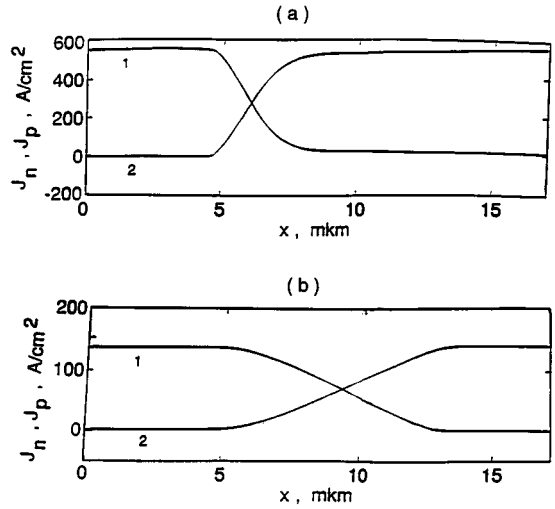

FIG. 5. Distributions of current for structure I at $t=4.5$ ns (a) and $t=14$ ns (b). The numbers 1 and 2 indicate hole and electron currents, respectively. Displacement current is negligible for $t\geqslant 2.5$ ns after reversing the anode voltage from 1 to -6 V.

(The last formula is valid in the region of high electric field, where the drift term is dominant and diffusion is negligible.) From Eq. (10) we obtain that hole concentration at $x=0$ decreases with time proportionally to the current $j(t)$:

$$p(x=0,t)=\frac{j(t)}{\mu_p(4\pi q^2/\epsilon)N_D a}\sim j(t), \tag{11}$$

what approximately corresponds to Figs. 2 and 4.

At the edge of the depletion region at $x=a$ the total current $j(t)\approx j_p(x,t)$, the hole current as can be seen from Fig. 5. Electron current j_n is negligible because of small number of electrons there. Using this, we can write for electric field at $x=a$:

$$E(a,t)=-\frac{kT}{q}\frac{1}{n(a,t)}\frac{\partial n}{\partial x}\bigg|_{x=a}. \tag{12}$$

Equation (12) means that electron drift and diffusion currents compensate each other at this point. Taking into account, that on the right of depletion region at $x\geqslant a$ $n(x,t)\approx p(x,t)$, it is easy to obtain, that the total hole current at the edge of the neutral region is equally distributed between drift and diffusion components as was first pointed out by Benda and Spenke[23] in the analysis of recovery problem in $p-i-n$ rectifiers:

$$qD_p\frac{\partial p}{\partial x}\bigg|_{x=a}=\frac{1}{2}\,j(t). \tag{13}$$

Gradient of hole distribution can be roughly estimated as an $dp/dx\approx\bar{p}(t)/W_n/2$, where W_n is the width of the n base, $\bar{p}(t)$ is the hole density in the space-charge region. Numerical analysis shows that this estimation is reasonable as soon as $\bar{p}(t)$ is at least ten times greater than impurity concentration. After this we have practically linear dependence of $p(x)$ in the whole n base. Assuming that $\bar{p}(t)\gg N_D$ we can write, that $j(t)\approx 2qD_p[\bar{p}(t)/W_n/2]$. It means, that $\bar{p}(t)$ also decreases proportionally to the total current $j(t)$. The latter is not a strong function of the applied voltage V. Taking into account Eq. (11) we obtain that the ratio $\bar{p}(t)/p(x=0,t)\approx 2q^2\pi N_D a/(\epsilon kT)\approx\sqrt{(V)}$. It does not depend on time and increases with the increase of applied voltage. For parameters used $N_d=10^{15}$ cm^{-3}, $kT=0.025$ eV, $V=6$ V, we obtain $\bar{p}(t)/p(x=0,t)\approx 4\times 10^3$, what on the order of magnitude corresponds to the curves in Fig. 2 and Fig. 4.

From the results of calculations for the ''wide'' structure it follows what is known experimentally: an attempt to pull out both electrons and holes by reversing anode voltage is not effective. Only electrons with a high mobility can be evacuated. The total voltage drop occurs across the space-charge region, which has been formed near the Pn junction. After this, the next slow period starts, when electric field is almost constant in the device, carrier concentrations gradually decrease. Part of the structure outside the depletion region remains quasineutral and is flooded by excess carriers, whose concentrations decrease proportionally to the current density $j(t)$, which is practically independent on the reverse

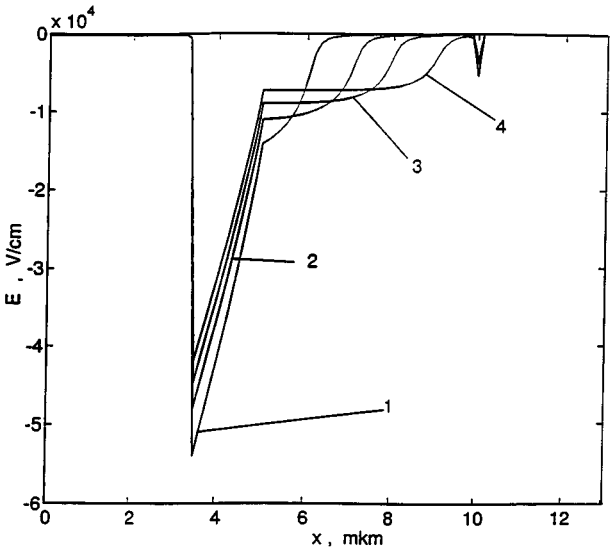

FIG. 6. Electric field at various moments of time t after applying the anode voltage -6 V to structure II. n and p bases have widths 1.5 and 5 μm, respectively. Doping concentrations are the same as in structure I. Total length of the structure is 13 μm. (1) $t=0.3$ ns, (2) $t=0.7$ ns, (3) $t=1.1$ ns, (4) $t=1.5$ ns.

applied voltage. Reverse recovery process for the structure I is a slow process, because electric field has little effect on the rate of holes removal.

B. "Narrow" base

Now we will consider another situation, when the width of n base is comparable with or less than the depletion region, formed after applying a negative anode voltage. In this case the n layer becomes completely depleted and is unable to consume all applied voltage. We call an n base "narrow" if its width W_n is less than the width of a space-charge region $a=\sqrt{\epsilon V/(2\pi qN_D)}$ at a given voltage V. Figures 6–9 show distributions of carriers and electric field at different moments of time after applying a negative voltage $V=-6$ V to the structure II at $t=0$. It is seen, that after a depletion region

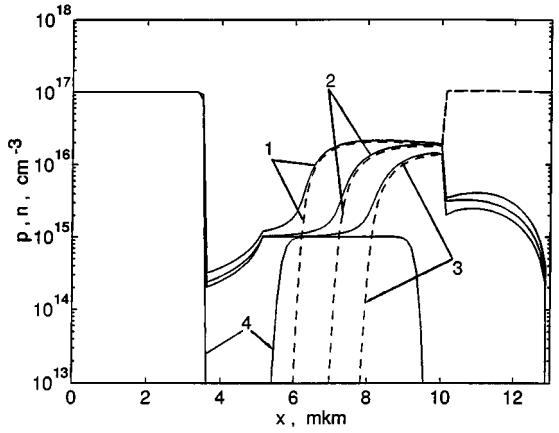

FIG. 7. Hole (solid lines) and electron (dashed lines) distributions for structure II. The numbers near the curves correspond to the following time moments: (1) $t=0.3$ ns, (2) $t=0.7$ ns, (3) $t=1.1$ ns. Curve 4 corresponds to the equilibrium hole distribution.

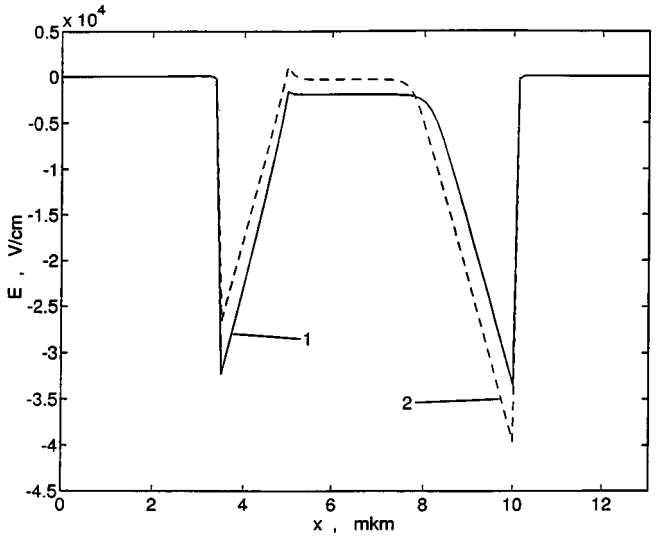

FIG. 8. Electric field in structure II at time moments when depletion region near the pN junction has been formed: (1) 1.7, (2) 1.9 ns.

has been formed near the Pn junction all n base is completely depleted and the field starts to penetrate into the p base. The boundary between n and p bases is then located at $x=5$ μm. In the second stage of reverse recovery process we can indicate three different regions in the device (Fig. 10): the depletion region I, which coincides now with the whole n base, and two neutral regions II and III. In the region II there is a constant electric field $E_0(t)$, electrons concentration is small and hole concentration has decreased up to the equilibrium level: $p=N_A$. The right boundary of this region $l_0(t)$ moves to the right, so that region III becomes narrower. In region III, electrons and hole densities $n(x,t)\approx p(x,t)\approx \bar{n}(x,t)$. The electric field is small in this region as well as the space charge. From Fig. 7 it is seen that at $t\approx 1.7$ ns the boundary between regions II and III reaches the pN junction. It means that at this moment all excess holes have been evacuated from the p base and the depletion region near the pN junction has been formed. At this moment of time the total current noticeably decreases (Fig. 12). Figures 8 and 9 demonstrate that at $t>1.7$ ns there are two depletion regions; the first is

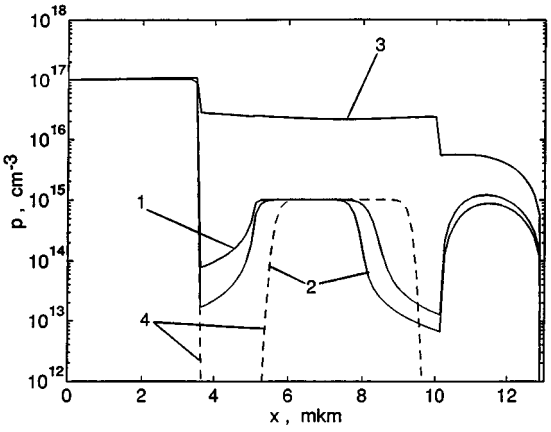

FIG. 9. Hole distribution for the same time moments (lines 1 and 2) as in Fig. 8. Curves 3 corresponds to the hole concentration in the ON state; curve 4 shows equilibrium hole distribution.

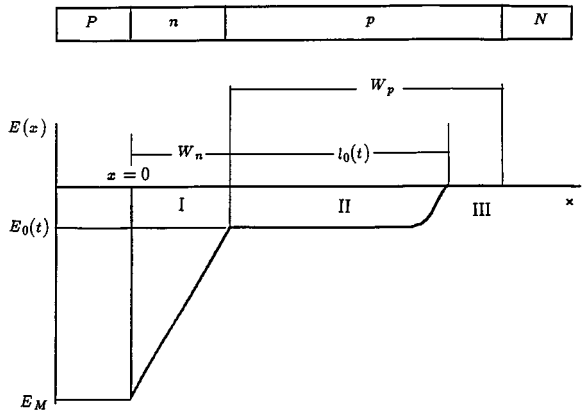

FIG. 10. Schematic plot of the electric field distribution $E(x)$ at some moment of time after the beginning of electric field penetration into the p base of structure II. n region (located at $0<x<W_n$) is completely depleted. In the region II hole concentration is equal to equilibrium value; electric field is $E_0(t)$. Excess holes and electrons are present only in the quasineutral region III. The boundary between regions II and III is located at $x=l_0(t)$ and moves to the right with the increase of time.

near the *Pn* and the second is near the *pN* junction. It means that in the regime of *n*-base punchthrough not only electrons, but also holes have been removed from the center regions of the device during a short period time $\approx$1.6 ns. After this process two outer junctions are reverse biased.

The time t_p, required for the electric field to go through the whole p base, determines the rate of removal of excess carriers from the device and, as we will see, is crucial for increase of immunity with respect to dV/dt switching. This increase was observed experimentally in Ref. 14. It is possible to get a closed expression for t_p. Poisson's equation in the completely depleted n region

$$\frac{\partial E(x,t)}{\partial x}=\frac{4\pi q}{\epsilon}N_D \tag{14}$$

can be integrated with the boundary condition $E(x=W_n)=E_0(t)$:

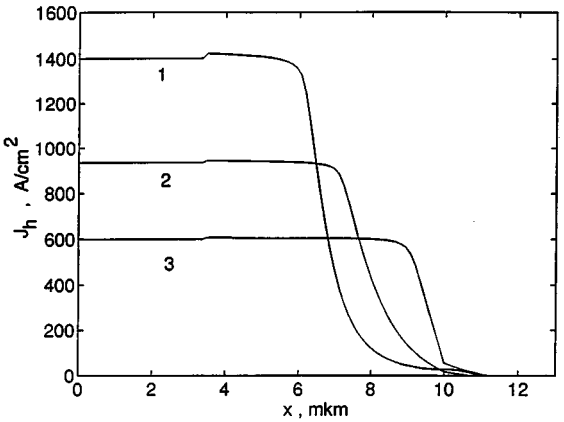

FIG. 11. Hole current J_h in structure II vs coordinate x at time moments: (1) 0.3, (2) 0.7, (3) 1.1 ns.

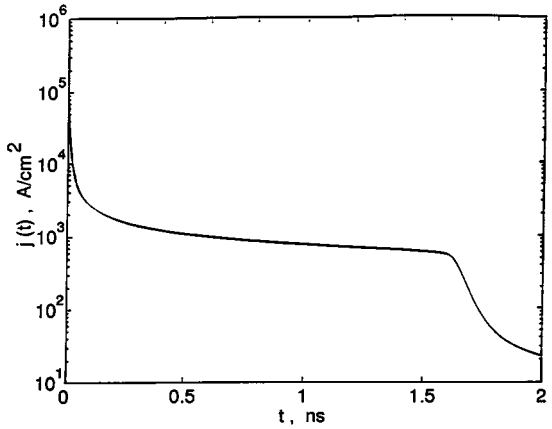

FIG. 12. Time evolution of the total particle current for structure II. At $t=0$ voltage V has been switched from $V=+1$ V to $V=-6$ V.

$$E(x,t)=\frac{4\pi q}{\epsilon}N_D(x-W_n)+E_0(t). \tag{15}$$

$E_0(t)$ is the electric field in region II. It is position independent, because the total current here is controlled by holes, whose concentration is equal to doping concentrations N_A:

$$j\approx j_p(t)=q\mu_p E_0(t)N_A. \tag{16}$$

Figure 11 shows that it is true up to the point $x=l_0(t)$. At $x=l_0(t)E_0(t)$ goes to zero. Assuming that its drop is abrupt after the second integration of the Poisson equation the voltage drop V across the device can be written as

$$V=\frac{E_M W_n}{2}+E_0(t)[l_0(t)+W_n], \tag{17}$$

where $E_M=(4\pi q/\epsilon)N_D W_n$.

The boundary $x=l_0(t)$ moves to the right with the velocity $|dl_0/dt|$. To get a relationship between $|dl_0/dt|$ and the current $j(t)$ we will integrate the hole continuity Eq. (3) over the p base:

$$\frac{\partial P}{\partial t}+\frac{j(t)}{q}=\int_0^{W_p}R(n,p)dx, \tag{18}$$

where P is the total number of holes in the p base, which can be written as

$$P=N_A l_0(t)+\bar{n}[W_p-l_0(t)]. \tag{19}$$

The right-hand part of Eq. (18) can be estimated as $B_0\bar{n}^2[W_p-l_0(p)]$. We will see below that this term is small and can be omitted. Using Eq. (18), we see that the boundary $x=l_0(t)$ moves to the right with the velocity $|dl_0/dt|$ so that the carrier content of the swept-out region just covers the current density $j(t)$:

$$j=q\bar{n}\left|\frac{dl_0}{dt}\right|=q\mu_p E_0(t)N_A. \tag{20}$$

To integrate the last equation we will assume that $\bar{n}=$const and after multiplying Eq. (20) by $[l_0(t)+W_n]$ and taking into account of Eq. (17), we get

$$l_0^2(t)+2l_0W_n=\frac{2\mu_p N_A}{\bar{n}}(V-V_0)(t-t_0), \tag{21}$$

where $V_0=E_MW_n/2=(2\pi q/\epsilon)N_DW_n^2$, t_0 is the moment of time, corresponding to the beginning of electric field penetration into the p base: $l_0(t_0)=0$.

Using Eq. (21), we can estimate the current density during the time interval $0<t<t_p$ when $l_0 \gg W_n$:

$$j(t)=q\bar{n}\frac{dl_0(t)}{dt}\sim q\sqrt{[\mu_p\bar{n}N_A(V-V_0)]/2t}\sim\frac{1}{\sqrt{t}}. \tag{22}$$

We can drop the last term in Eq. (18) if

$$\frac{qB_0\bar{n}^2[W_p-l_0(t)]}{q\bar{n}dl_0(t)/dt}<\frac{B_0\bar{n}W_p}{W_p/t_p}=B_0\bar{n}t_p\ll 1. \tag{23}$$

The time t_p necessary for electric field to reach the pN junction [when $l_0(t)=W_p$], is given by

$$t_p=t_0+\frac{1}{2}\frac{\bar{n}}{N_A}\frac{W_p^2+2W_pW_n}{(V-V_0)\mu_p}. \tag{24}$$

Substituting into this expression the values $N_A=N_D=10^{15}$ cm^{-3}, $\bar{n}=2\times10^{16}$ cm^{-3}, $W_p=5\times10^{-4}$ cm, $W_n=1.5\times10^{-4}$ cm^{-3} gives $V_0=1.85$ V and for $V=6$ V we obtain $t_p\approx2.1$ ns. It is in good agreement with Figs. 8 and 9. Substitution of numerical values into Eq. (23) shows that the process of electric field penetration is fast enough, so Eq. (23) holds: $B_0\bar{n}t_p\approx0.03\ll1$.

C. Immunity with respect to *dV/dt* switching

It is well known experimentally that a fast increase of the anode voltage induces switching of a thyristor before a quasistatic break-over voltage is reached. It was pointed out in Ref. 14, that the remaining majority carriers (holes in the p base) supporting the ON state, provide a forward bias for the emitter-base pN junction and induce dV/dt switching. To reveal the effect of electric field penetration into the p base we have performed a transient simulation for the applied anode voltage, which has the following form. Starting from the positive value $V=0.5$ V, the anode voltage V is pulsed to a negative value $V_{\rm neg}$. After an interval of time $T_{\rm neg}$ the voltage V increases during 1 ns to the value $V_{\rm pos}$.

Maximum positive voltage $V_{\rm pos}^{\rm max}$, up to which the thyristor can be pulsed in 1 ns without switching on, is plotted as a function of $T_{\rm neg}$ in Fig. 13. For negative voltages $V<V_0$, small positive bias switches the device ON and this positive bias practically does not depend on the magnitude $T_{\rm neg}$. For $V>V_0$ immunity sharply increases for $T_{\rm neg}\approx t_p$. This shows that t_p, calculated in the previous section, has a meaning of a switching time of our device. $V_{\rm pos}^{\rm max}$ practically does not depend on the magnitude of $T_{\rm neg}$ for $t>T_{\rm neg}$.

IV. CONCLUSION

We have developed a numerical model for an analysis of reverse recovery processes in optoelectronic thyristors. Results of numerical calculations demonstrate, that there are two substantially different regimes of a recovery process. For small reverse voltages the depletion region is formed near the anode, p-base junction as a result of removal of fast diffusing electrons. After the depletion region is formed, the tail period starts and electron and hole concentrations gradually decrease with time. The depletion region takes most of the applied voltage. The electric field is not efficient from the viewpoint of removal of slow diffusing holes.

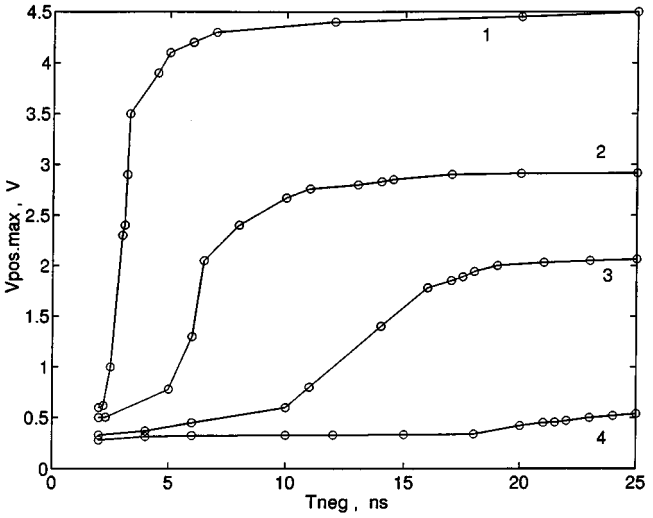

FIG. 13. Maximum positive voltage $V_{\rm pos,max}$, up to which the thyristor can be pulsed in 1 ns without switching on vs $T_{\rm neg}$. $T_{\rm neg}$ is the time interval, during which a negative voltage $V_{\rm neg}$ was applied. Curves 1, 2, 3, 4 correspond to $V_{\rm neg}=-4.5$, -3.5, -2.5, and -0.5 V.

In the regime of punchthrough, when the n base is sufficiently narrow, the space-charge region near the Pn junction is unable to consume all negative applied voltage. After the n layer becomes completely depleted, the electric field starts penetrating into the p base and enhances removal of holes. Rate of this penetration and recovery time has been calculated in terms of device parameters. For narrow n bases, time t_p, required to evacuate all excess holes from the center region, is proportional to the square of the p-base width. Immunity with respect to dV/dt switching sharply increases if a thyristor is kept under the negative voltage longer than t_p. The numerical model allows to see the main features of the reverse recovery processes in optothyristors in the regime of n-base punchthrough and it may be helpful for a design of fast switches, based on two-terminal optoelectronic thyristors.

ACKNOWLEDGMENT

This work was supported by ARO.

[1] G. Taylor, J. Simmons, A. Cho, and R. Mand, J. Appl. Phys. **59**, 596 (1986).
[2] J. Simmons and G. Taylor, IEEE Trans. Electron. Devices **ED-35**, 1278 (1988).
[3] G. Taylor and P. Cooke, IEEE Trans. Electron. Devices **ED-39**, 2529 (1991).
[4] W. Shou-Wu, W. Rong-Han, Z. Quan-Sheng, and H. Dan-Xia, Solid-State Electron. **30**, 53 (1987).
[5] W. Crawford, G. Taylor, P. Cooke, T. Y. Chang, B. Tell, and J. Simmons, Appl. Phys. Lett., **53**, 1797 (1988).
[6] D. Crawford, G. Taylor, and J. Simmons, Appl. Phys. Lett. **52**, 863 (1988).
[7] A. Sasaki, S. Metavikul, M. Itog, and Y. Takeda, IEEE Trans. Electron. Devices **ED-35** (1988).

[8] K. Kasahara, Y. Tashiro, N. Namao, M. Sugimoto, and T. Yanase, Appl. Phys. Lett. **52**, 679 (1988).
[9] S. Wang, Q. Zhu, Q. Zhang, Z. Li, and H. Tian, IEEE Proc. 1, Solid State Electron Devices **129**, 306 (1982).
[10] O. A. Belyaeva, S. N. Vainstein, Yu. V. Zhilyaev, M. E. Levinstein, and V. E. Chelnokov, Sov. Tech. Phys. Lett. **12**, 383 (1986).
[11] S. M. Sze, *Physics of Semiconductor Devices* (Wiley, New York, 1981), pp. 613–618.
[12] Y. Tashiro, K. Kasahara, N. Hamao, M. Sugimoto, and T. Yanase, Jpn. J. Appl. Phys. **26**, L1014 (1987).
[13] P. Heremans, M. Kuijk, and G. Borghs, IEDM Tech. Dig. **91**, 433 (1983).
[14] P. L. Heremans, M. Kuijk, and G. Borghs, Appl. Phys. Lett. **61**, 1326 (1992).
[15] H. Z. Fardi, IEEE Trans. Comput.-Aided Design Integr. Circuit. Syst. **12**, 666 (1994).
[16] B. J. Baliga, *Power Semiconductor Devices* (PWS, Boston, 1994), Chap. 6.
[17] R. Olshansky, C. B. Su, J. Manning, and W. Powazinic, IEEE J. Quantum Electron. **QE-20**, 838 (1984).
[18] S. Selberherr, *Analysis and Simulation of Semiconductor Devices* (Springer, Berlin, 1984).
[19] D. L. Scharfetter and H. K. Gummel, IEEE Trans. Electron. Devices **ED-16**, 64 (1969).
[20] S. C. Eisenstat, M. C. Gursky, M. H. Schultz, and A. N. Scherman, Tech. Rep. 14, Yale University, 1977.
[21] M. Kurata, *Numerical Analysis for Semiconductor Devices* (Heath, Boston, 1982).
[22] M. S. Adler, D. N. Pattnayak, B. J. Baliga, V. A. K. Temple, and H. R. Chang, Proceedings of the Fifth International Conference on the Numerical Analysis of Semiconductor Devices and Integrated Circuits, 17–19 June 1987, pp. 1–19.
[23] H. Benda and E. Spenke, Proc. IEEE **55**, 1331 (1967).